

1
2
3
4
5
6
7
8
9
10
11
12
13
14
15
16

Sources and pathways of glacial meltwater in the Bellingshausen Sea, Antarctica

Peter MF Sheehan¹, Karen J Heywood¹,
Andrew F Thompson², M Mar Flexas² and Michael P Schodlok³

¹Centre for Ocean and Atmospheric Sciences, School of Environmental Sciences, University of East Anglia, Norwich, United Kingdom
²Environmental Science and Engineering, California Institute of Technology, Pasadena, California, United States
³Jet Propulsion Laboratory, California Institute of Technology, Pasadena, California, United States

Key Points:

- Meltwater pathways in the Bellingshausen Sea, Antarctica, are explored using observations from gliders and a high-resolution regional model
- Meltwater observed at different densities originates from different ice shelves: lighter meltwater layers originate from eastern ice shelves
- Meltwater from different ice shelves is distinguished by different turbidity signatures, suggestive of different biogeochemical properties

Corresponding author: Peter Sheehan, p.sheehan@uea.ac.uk

Abstract

Meltwater content and pathways determine the impact of Antarctica’s melting ice shelves on ocean circulation and climate. Using ocean glider observations, we quantify meltwater distribution and transport within the Bellingshausen Sea’s Belgica Trough. Meltwater is present at different densities and with different turbidities: both are indicative of a layer’s ice shelf of origin. To investigate how ice-shelf origin separates meltwater into different export pathways, we compare these observations with high-resolution tracer-release model simulations. Meltwater filaments branch off the Antarctic Coastal Current into the southwestern trough. Meltwater also enters the Belgica Trough in the northwest via an extended western pathway, hence the greater observed southward (0.50 mSv) than northward (0.17 mSv) meltwater transport. Together, the observations and simulations reveal meltwater retention within a cyclonic in-trough gyre, which has the potential to promote climactically important feedbacks on circulation and future melting.

Plain-language summary

Recent research has advanced our understanding of interactions between warm ocean waters and the underside of Antarctica’s floating ice shelves. But what happens to meltwater that these ice shelves release? Meltwater is fresh: it reduces the salinity of sea water and upsets the delicate balance between salty and fresh water that drives many polar ocean processes – for example the sinking of cold, salty water to the deepest regions of the ocean, which is of global climatic importance. We use high-resolution observations and state-of-the-art model simulations to determine the pathways that meltwater takes as it flows in and around the Belgica Trough in the central Bellingshausen Sea, Antarctica. Meltwater is principally confined to the edges of the trough’s clockwise gyre circulation. Meltwater from eastern ice shelves is generally found at shallower depths than meltwater from southern ice shelves; this explains evidence of two meltwater layers found in our observations. In addition, meltwater from eastern ice shelves is turbid, while meltwater from southern ice shelves is clear. These results will help us to better predict how Antarctica’s coastal seas will respond to a warming climate as ever more meltwater is released into the ocean.

1 Introduction

The intrusion of warm Modified Circumpolar Deep Water (mCDW; $\sim 1.2^\circ\text{C}$, $\sim 34.6\text{ g kg}^{-1}$; Whitworth et al., 1998) onto the continental shelf of West Antarctica – that is, along the western coast of the Antarctic Peninsula and in the Bellingshausen and Amundsen Seas (Figure 1a) – contributes to melting of the region’s glaciers and ice shelves (Wählín et al., 2010; Jenkins et al., 2018). Aided by the proximity of the Antarctic Circumpolar Current to the shelf break (Orsi et al., 1995), ocean and atmospheric processes control the delivery of mCDW to the ice front (e.g. Moffat et al., 2009; Kimura et al., 2017; Gunn et al., 2018; Nakayama et al., 2018; Kim et al., 2021; Oelerich et al., 2022). Widespread mCDW intrusions make sea floor temperatures over West Antarctica’s continental shelf the warmest of all Antarctica’s shelf seas (Thompson et al., 2018); the glaciers and ice shelves that meet these warm waters are the fastest melting on the continent (Rignot et al., 2019).

Glacial meltwater (i.e. fresh water derived from basal melting of ice shelves; “meltwater” hereafter) from mCDW-induced basal melting is injected at depth, but can rise to the surface if sufficiently buoyant given local stratification (Zheng et al., 2021). Meltwater can circle the continent (Nakayama et al., 2020) and modify ocean stratification, thus altering geostrophic circulation, vertical mixing and vertical and lateral heat fluxes. Transport of meltwater to deep-water formation sites, such as the

66 Ross Sea, can alter the properties and formation rates of water masses that ventilate
67 the abyssal ocean (Jacobs & Giulivi, 2010; Silvano et al., 2018; Lago & England,
68 2019). Circulation and stratification changes induced by the addition of meltwater can
69 alter ice-shelf melt rates (Donat-Magnin et al., 2017; Flexas et al., 2022), even if the
70 meltwater injection occurs far from the ice shelf. Quantifying meltwater content over
71 the Antarctic continental shelf, and describing its pathways and origins, is therefore key
72 to understanding the impact of a warming, melting Antarctica on ocean circulation.

73 The Bellingshausen Sea is poorly observed, general features of the circulation hav-
74 ing been elucidated only recently and with sparse observations (e.g. Jenkins & Jacobs,
75 2008; Zhang et al., 2016; Thompson et al., 2020; Ruan et al., 2021; Schulze Chretien
76 et al., 2021). Two major troughs are present: Belgica Trough in the west and Latady
77 Trough in the east (Figure 1b). As elsewhere, these troughs, both of which host cy-
78 clonic circulations (Zhang et al., 2016; Schulze Chretien et al., 2021), appear to be
79 the principal conduits by which mCDW transits the continental shelf and accesses the
80 ice shelves (Ruan et al., 2021; Schulze Chretien et al., 2021). Flow in the troughs is
81 largely barotropic (Schulze Chretien et al., 2021). Meltwater has been observed across
82 the Bellingshausen (Zhang et al., 2016), but there is evidence that it is concentrated in
83 the northward flowing limbs of the troughs' cyclonic gyres (Zhang et al., 2016; Ruan
84 et al., 2021; Schulze Chretien et al., 2021). Meltwater that reaches the shelf break is
85 thought to exit the Bellingshausen via westward-flowing shelf-break currents, although
86 evidence for this is less certain (Zhang et al., 2016; Thompson et al., 2020). Quanti-
87 fying the meltwater circulation in all limbs of the troughs' circulation at a resolution
88 sufficient to capture the small Rossby deformation radius at high latitudes would en-
89 able a more complete understanding of the role of meltwater in driving hydrographic
90 and circulation changes in this rapidly warming region.

91 Here, we use novel ocean glider observations to estimate the glacial meltwater
92 content in, and its transport around, Belgica Trough. Unlike previous ship-based
93 surveys, the high horizontal resolution of our observations allows us to resolve the
94 narrow boundary currents of the trough circulation for the first time. We perform
95 tracer release experiments using a regional model to separate the pathways taken by,
96 and density ranges occupied by, meltwater originating from the principal ice shelves of
97 the Bellingshausen Sea's perimeter. Given the large difference in melt rates between
98 the region's various ice shelves (Rignot et al., 2019), investigating this question should
99 help elucidate future changes in the hydrography of the Bellingshausen Sea, and help
100 refine projections of how attendant circulation changes might occur.

101 2 Methods

102 We analyse temperature, salinity, optical backscatter and dive-average current (Frajka-
103 Williams et al., 2011; Garau et al., 2011; Green et al., 2014) observations collected by
104 a Seaglider deployed in the Bellingshausen Sea (Lee et al., 2022). The glider occupied
105 on-shelf and cross-slope transects between 1 February and 20 March 2020; we present
106 observations from six on-shelf transects (Figure 1b), with each transect lasting four
107 to five days. We use the glider's temperature and salinity observations (Figure S1)
108 to calculate meltwater concentration following the method of Jenkins (1999), see also
109 Biddle et al. (2017) and Zheng et al. (2021). Characteristic core temperature and
110 salinity values of mCDW, WW and meltwater are defined (Table S1); the meltwater
111 content of an observation is then determined by quantifying the deviation, in the
112 direction of pure meltwater, of that observation from the mCDW-WW mixing line in
113 temperature-salinity space (Jenkins, 1999). The total geostrophic current, comprising
114 the glider-derived geostrophic shear and a reference velocity based on the glider's de-
115 tided (Padman et al., 2002, 2008) dive-averaged current, is used to estimate meltwater
116 transport. A comprehensive description of the glider observations and the meltwater
117 calculation method is presented in the supporting information.

118 To investigate sources and pathways of meltwater, we perform high-resolution
 119 tracer release experiments using the Massachusetts Institute of Technology general
 120 circulation model, full details of which are given by Flexas et al. (2022). The model
 121 domain, which comprises the Amundsen and Bellingshausen Seas, is derived from the
 122 global configuration (LLC1080) used by the Estimating the Circulation and Climate
 123 of the Ocean project (ECCO; Forget et al., 2015) with a horizontal grid spacing of
 124 approximately 3 km. Initial and boundary conditions are derived from a global state
 125 estimate (ECCO LLC270); surface forcing is taken from ERA5 (Hersbach et al., 2020).
 126 Outputs are given as daily means. We present a comparison of the observations and
 127 model output in the supporting information.

128 Tracers were released at a concentration of 1 kg kg^{-1} at all grid points within
 129 the nine ice shelf cavities of the Bellingshausen Sea perimeter on the first day of each
 130 month between August 2019 and July 2020 (inclusive). Separate tracers were released
 131 under each ice shelf in order that the resulting tracer distributions might be considered
 132 individually. Tracer concentration is not the same as meltwater concentration, which
 133 would be greatest at the ice-ocean interface. Tracer concentration more accurately
 134 represents ice shelf cavity water; while it cannot be used to quantify meltwater con-
 135 centration, it is used here as a proxy for identifying meltwater pathways. We present
 136 results from the August 2019 release averaged over March 2020, i.e. the time of the
 137 glider observations. We focus on tracers from the George VI and Venable ice shelf
 138 cavities.

139 We calculate the tracer-weighted mean density, $\bar{\sigma}$ (kg m^{-3}). We first calculate
 140 tracer mass, M (kg), in a given grid box, then calculate $\bar{\sigma}$ according to:

$$\bar{\sigma} = \int_{-H}^0 M \sigma dz / \int_{-H}^0 M dz, \quad (1)$$

141 where H is the depth of the seafloor (m) and z is depth (m). Finally, we calculate the
 142 mean of $\bar{\sigma}$ over each month.

143 3 Glider observations of meltwater and meltwater transport

144 The glider’s dive-average currents (Figure 1) confirm the cyclonic gyre circulation
 145 inside Belgica Trough described by previous studies (e.g. Schulze Chretien et al.,
 146 2021). There is a narrow band of northward flow in the southwest, in the vicinity
 147 of the 500 m isobath; we interpret this as the gyre’s western boundary flow. Flow is
 148 approximately eastward to the immediate south of the shelf break; and there are two
 149 jets of generally southward flow in the central and eastern Trough, in water deeper than
 150 600 m (Figure 1b). We do not observe the putative westward flow in the south that
 151 would be necessary to close the gyre circulation, likely because the glider sections do
 152 not extend sufficiently far south to reach the coast. To the east (84°W), in the shallower
 153 water between the Belgica and Latady troughs, there is also an approximately eastward
 154 flow to the south of the shelf break (Figure 1b); this suggests that the eastward flow
 155 within the trough may be a combination of a shelf-break feature and the trough’s gyre
 156 circulation.

157 We observe net southward meltwater transport within Belgica Trough. In the
 158 north, two cores of pronounced eastward flow transport meltwater approximately par-
 159 allel to the shelf break (Figure 2a). Depth-integrated meltwater content in this north-
 160 ern region exceeds 0.35 m (Figure 1b, where depth-integrated meltwater content is the
 161 product of meltwater concentration and bin-thickness, summed over a profile); inte-
 162 grated meltwater transport is 0.67 mSv (i.e. meltwater transport integrated over all
 163 depths between 30 and 70 km along transect one; $1 \text{ mSv} = 10^{-3} \text{ Sv}$). In the central
 164 and eastern trough, two meltwater cores, each approximately 30 km wide, flow south-

ward (Figure 2e). Depth-integrated meltwater content in these flows is approximately 0.3 m (Figure 1b); integrated meltwater transport is 0.50 mSv (0 to 80 km along transect five). The principal meltwater flow in the trough’s western boundary current is limited in horizontal extent, being confined to a relatively narrow (10 km) northward-flowing core in the southwest (Figures 1b and 2e). Integrated meltwater transport is 0.17 mSv (0 to 25 km along transect three). In the shallow region between Belgica and Latady Troughs, outside Belgica Trough’s gyre circulation, meltwater concentrations are relatively low ($< 1 \text{ g kg}^{-1}$; Figure 2e and f). The sharp boundary between the two regimes can be seen approximately 80 km along transect five (Figure 2e). We note that the glider transects may have been too short to capture the full width of the various flows, particularly in the southwest (transect three); our observations may therefore under-estimate the total meltwater transport.

Meltwater layers in Belgica Trough are centered on different density classes in different places, and the thickness of the meltwater layer varies spatially (Figure 2). In the northern and eastern trough, meltwater is present in an approximately 200 m-thick layer centered on the 27.7 kg m^{-3} isopycnal (Figure 2a and e). In the western trough, meltwater is present in an approximately 100 m-thick layer centered on and immediately below the 27.6 kg m^{-3} isopycnal (Figure 2b, c and d). Around the center of the trough, a similarly thin (100 m) meltwater layer is present between the 27.5 and 27.6 kg m^{-1} isopycnals (Figure 2b and d).

Meltwater layers in Belgica Trough may be distinguished by their turbidity. The turbidity of the thick, high-meltwater flows in the northern and central trough is indistinguishable from that of the surrounding water (Figure 2a and e, open arrows in Figure 1b). In contrast, meltwater in the western boundary current is more turbid than the surrounding water (Figure 2b and c, filled arrow in Figure 1b). We note that the vertical extent of the high-turbidity regions associated with the western meltwater flows is greater than the vertical extent of the meltwater flows themselves. This is a consequence of our choosing core temperature and salinity values of mCDW and WW that produce conservative estimates of meltwater. Using less conservative core temperature and salinity values of mCDW and WW (e.g. from transect three) increases the vertical extent over which meltwater is found and improves the spatial correlation between meltwater and turbidity (Figure S6). The distinct optical properties suggest that the two meltwater layers either originate from different ice shelves with different sediment loads, or that they originate from different locations such that their sediment load has had longer to be deposited en route.

200 **4 Sources and pathways of glacial meltwater**

We turn to model simulations and tracer release experiments to investigate pathways of meltwater within the Bellingshausen, as well as the provenance of meltwater in Belgica Trough. Tracers released under both George VI and Venable ice shelves are present within the gyre circulation of Belgica Trough seven months after release, i.e. in March 2020 at the time of the glider observations (Figure 3; similarly to Figure 1b, we plot depth-integrated tracer content, i.e. the product of tracer concentration and bin-thickness, summed over a profile). Tracer released under George VI ice shelf that exits the cavity via its northern opening (70°S , 70°W) is advected southwards in the eastern Bellingshausen (Figure 3a and f). Tracer that exits the George VI cavity via the southern opening (73°S , 72°W) is advected westward by the Antarctic Coastal Current (Schubert et al., 2021) and is, east of 85°W , largely confined to the coast (Figure 3a and f). West of approximately 90°W – that is, to the west of Belgica Trough – George VI tracer spreads northwards across the continental shelf, eventually reaching the shelf break (Figure 3a and f). All tracer released under Venable ice shelf is transported westward, spreading over the western Bellingshausen from the ice edge to the shelf break (Figure 3b). This generally westward tracer transport is a

217 common feature of simulations of the Bellingshausen Sea (Nakayama et al., 2014, 2017;
 218 Dawson et al., 2023). Nakayama et al. (2014) show that, after a 10-year simulation,
 219 westward export tends to be concentrated to the south of the shelf break; in our
 220 year-long simulation, tracers first reach the western Bellingshausen in the Antarctic
 221 Coastal Current, before spreading northwards to the shelf break over the ensuing
 222 months (Figures 3 and S8).

223 In the southwestern Belgica Trough, a narrow filament of tracer flows north-
 224 ward, towards the shelf break, in the region of the trough’s western-boundary current
 225 (Figure 3a and b); we observe northward meltwater transport in this same feature
 226 (Figures 1 and 2c). The northward-flowing filament branches off from a small (i.e.
 227 80 to 100 km across) cyclonic gyre feature immediately to the north of Venable; this
 228 Venable gyre itself draws tracer from the Antarctic Coastal Current at approximately
 229 89°W , and tracer from both ice shelves circulates within it (Figure 3a and b). To the
 230 east, a second tongue branches off the Venable gyre and follows the 500 m isobath into
 231 the south-central Belgica Trough; this is particularly apparent in the distribution of
 232 the Venable tracer (Figure 3b).

233 Not all meltwater found in Belgica Trough flows into the trough from the south.
 234 Instead, Venable tracer flows into Belgica Trough in the northwest, having first spread
 235 over the western Bellingshausen. An eastward-flowing filament of tracer from Venable
 236 enters Belgica Trough at approximately 71°S (Figure 3b and f). The beginnings of
 237 such an eastward filament can be seen in tracer from George VI: this filament reaches
 238 the northern Belgica Trough in subsequent months (Figure S8). High meltwater con-
 239 centrations and high meltwater transport are present in this eastward flow in the glider
 240 observations (Figure 2b).

241 Tracer from Venable is also present in the central and eastern Belgica Trough, in
 242 the region of the two cores of southward meltwater transport seen in the observations
 243 (Figures 2, 3b and S10). Again, tracer from George VI is absent from this region
 244 in March 2020, but is present in subsequent months (Figure S8). The concentra-
 245 tion of Venable tracer in this region increases in subsequent months, and the filament
 246 penetrates further southward (Figure S8). As in the western Belgica Trough, tracer
 247 re-circulating in the eastern trough largely remains in waters deeper than 500 m (Fig-
 248 ure 3d). This agrees with our observations of this southward flow (Figures 1b and 2e):
 249 meltwater concentrations are high in the southward flow within the trough, and lower
 250 outside the trough’s cyclonic gyre, i.e. in the shallower region between Belgica and
 251 Latady troughs.

252 We calculate the cumulative sum of tracer mass, as a percentage of the total
 253 mass of tracer released, that crosses: a meridional section at 86°W , between 70 and
 254 71°S (i.e. the eastward flow in the northern Belgica trough); and a zonal section at
 255 71°S , between 83 and 86°W (i.e. the southward re-circulation). Over the year-long
 256 simulation, 0.6% of the George VI total tracer mass crosses the meridional section,
 257 and 0.3% crosses the zonal section. Of the Venable tracer, 4.7% crosses the meridional
 258 section and 3.1% crosses the zonal section.

259 Tracers from George VI and Venable ice shelves predominate at different mean
 260 densities, $\bar{\sigma}$, within the Bellingshausen Sea. In the southwestern Belgica Trough, as
 261 across the western Bellingshausen, tracer from George VI is found at mean densi-
 262 ties between approximately 27.4 and 27.6 kg m^{-3} (Figure 3c); tracer from Venable is
 263 found at greater mean densities: between approximately 27.6 and 27.8 kg m^{-3} (Fig-
 264 ure 3d). This density difference of approximately 0.1 to 0.2 kg m^{-3} in the western
 265 Bellingshausen is broadly consistent over time (not shown). In both the northern and
 266 eastern Belgica Trough, the difference between the mean densities of the George VI
 267 and Venable tracers is, in places, close to zero (Figure 3e). This qualitative pattern is
 268 consistent for tracer released in all months (not shown). The fact that tracer originat-

269 ing under Venable is found on denser isopycnals than tracer from under George VI may
270 explain why the former penetrates the cavities under western ice shelves such as Ab-
271 bot, whereas the latter, higher in the water column, remains in open water (Figure 3a
272 and b).

273 The mean densities of tracer from George VI, in the eastern Bellingshausen, and
274 Venable, in the southern Bellingshausen, are representative of the mean densities of
275 tracer released under the other ice shelf cavities of the eastern and southern Belling-
276 shausen respectively: in Belgica Trough and across the western Bellingshausen Sea,
277 tracer from eastern ice shelves (i.e. George VI, Wilkins and Bach) is found at lesser
278 mean densities (i.e. shallower) than tracer from southern ice shelves (i.e. Venable and
279 Ferrigno). This modelling result is consistent with the difference between the density
280 of meltwater layers that we observe in Belgica Trough. Relatively dense meltwater
281 layers, such as that observed in the northern and western trough ($\geq 27.7 \text{ kg m}^{-3}$; Fig-
282 ure 2a and e) contain meltwater from southern ice shelves; relatively light meltwater
283 layers, such as those observed in the southwestern trough ($\leq 27.6 \text{ kg m}^{-3}$; Figure 2b
284 and c) contain meltwater from eastern ice shelves.

285 We may now synthesize results from the observations and the modelling exper-
286 iments in a schematic of meltwater transport in the Bellingshausen Sea (Figure 3f).
287 While the model suggests that tracers from the ice shelves of the eastern and south-
288 ern Bellingshausen enter Belgica Trough in the southwest, i.e. from the small gyre
289 immediately north of Venable Ice Shelf (orange in Figure 3), we observe only lighter
290 meltwater flowing northward in the western boundary current (Figure 2b and c). Con-
291 sequently, we conclude that meltwater in the western boundary current originates from
292 the eastern Bellingshausen (e.g. George VI). Furthermore, meltwater from the eastern
293 Bellingshausen would therefore appear to be responsible for the high-turbidity signal
294 in the observations. Meltwater observed in the northern and western Belgica Trough
295 is present in a thicker, lighter layer, and is of low turbidity. These differences suggest
296 a different origin to the denser, more turbid meltwater layer observed in the western
297 Bellingshausen; the model results suggest that meltwater in the northern and west-
298 ern Belgica Trough originates from the southern Bellingshausen (e.g. Venable). We
299 note that the model indicates a pathway for dense Venable meltwater via the western
300 boundary current (Figure 2b); this is not observed, but its absence may be due to
301 temporal variability that we miss with a single glider transect, or else due to spatially
302 incomplete observations because the glider did not go south to the coast because of
303 sea-ice coverage. Nevertheless, the lack of dense Venable-origin meltwater observed
304 in the western boundary current invites speculation on an alternative pathway be-
305 tween Venable and the northwestern Belgica Trough: the tracer results suggest that
306 this is via the western Bellingshausen (Figure 3). And since high-turbidity meltwa-
307 ter in Belgica Trough originates from further away than low turbidity-meltwater, we
308 discount the hypothesis that the difference is due to high-turbidity meltwater having
309 been transported further from its source, depositing its sediment load en route; rather,
310 meltwater from different ice shelves must have different initial sediment loads. This
311 result may have important implications for the potential injection of iron, and other
312 micro-nutrients and tracers into the Bellingshausen.

313 5 Discussion and conclusions

314 Small-scale gyres are common features of the Antarctic continental shelf (e.g. Zheng
315 et al., 2022), and they create the conditions in which meltwater re-circulations can
316 occur. Given the influence of meltwater on the strength of the shelf circulation (e.g.
317 Thurnherr et al., 2014), retention and re-circulation have the potential to induce posi-
318 tive feedbacks. For instance, increased melting can strengthen the on-shelf overturning
319 circulation via water mass transformation, but advection of meltwater also influences
320 the on-shelf density structure that determines the horizontal geostrophic circulation

(Thompson et al., 2020). Both overturning and horizontal circulations influence the delivery of mCDW to the ice front, potentially allowing for ice-shelf melt feedbacks. Furthermore, an increase in meltwater-induced stratification in southward flows, which are responsible for the delivery of mCDW to the ice-front, could suppress the upward mixing of heat out of the mCDW layer (Flexas et al., 2022); warmer mCDW would then reach the ice front. Therefore, in addition to examining the far-field transport of West Antarctic meltwater and its downstream influence (e.g. Silvano et al., 2018; Lago & England, 2019), future work should consider to the local influence of meltwater build-up within in-trough gyres. Further, we note that our simulated pathways are strongly dependent on model bathymetry. Given the relative lack of ship-based bathymetry in the Bellingshausen Sea (although instrumented seals have been used to improve coverage; Padman et al., 2010), additional meltwater pathways may exist; these pathways, and their contribution to retention and re-circulation, could usefully be re-examined in future as bathymetry products improve.

We show that meltwater originating from different ice shelves becomes neutrally buoyant at different densities: meltwater from ice shelves in the eastern Bellingshausen becomes neutrally buoyant at lighter densities than meltwater from ice shelves in the southern Bellingshausen. The average density of meltwater from George VI and Venable decreases with distance from each ice shelf (Figure 2c and d), consistent with its mixing predominantly with lighter waters above. We also note that, at the ice front, in the model as in reality, the draft of Venable (280 m) is deeper than the draft of George VI (65 m in the north, 165 m in the south; Morlighem et al., 2020); indeed tracer from Venable is injected at greater densities than tracer from George VI (Figure 2c and d). Alongside the markedly different observed turbidity signatures of meltwater originating from the ice shelves of the eastern and southern Bellingshausen this suggests that the density of a meltwater layer may point to its origin. Observations of meltwater in cavity outflows would help determine whether, in the real ocean, the density of a meltwater layer is largely set by the density at which it exits a cavity; and observations of turbulence over the Antarctic continental shelf would help determine the importance of downstream mixing in altering the initial density of a layer.

Meltwater released by ice shelves in one region may influence the circulation of the Antarctic continental shelf in different ways to meltwater released elsewhere. The volume of meltwater released by a given ice shelf, and the corresponding change in the stratification, may alter the density at which meltwater released downstream becomes neutrally buoyant. Differences in meltwater turbidity, which we propose are indicative of differences in turbidity at the original ice shelves, suggest that biogeochemical processes influenced by meltwater may be sensitive to the ice shelf from which a given meltwater sample originates. An increase in the melt rate of one ice shelf may therefore have a different physical and biogeochemical influence on Antarctica's continental shelf seas than the same increase in the melt rate of another ice shelf. Together, this suggests that not all meltwater is created equal: a full understanding of the influence of meltwater on the Antarctic continental shelf requires a quantitative understanding of the melt rate of individual ice shelves and the subsequent transport pathways of individual meltwater layers. Furthermore, an intricate system of small-scale gyres and boundary currents over the continental shelf determines the large-scale distribution of meltwater. The resulting distribution will play a large role in determining meltwater's overall influence on the circulation, both locally and downstream. Characterization of variability in these circulation features and their impact on ocean-ice interactions remains an under-explored but important research direction.

Data availability

The Seaglider observations (Lee et al., 2022) used in this study are archived at the British Oceanographic Data Centre (*bodc.ac.uk*) with the DOI:

373 10.5285/ea24b8e5-b10e-68bf-e053-6c86abc06c97. MITgcm and its user manual are
 374 available at: mitgcm.org/ and the source code may be downloaded from:
 375 github.com/MITgcm/MITgcm. Information on the ECCO LLC270 ocean-ice state es-
 376 timate is available at: hdl.handle.net/1721.1/119821 and instructions for its download
 377 are available at: ecco-group.org/products-ECCO-V4r4.htm. The ERA5 re-analysis is
 378 available from the ECMWF
 379 (ecmwf.int/en/forecasts/datasets/reanalysis-datasets/era5), and instructions for its down-
 380 load are available at: confluence.ecmwf.int/display/CKB/How+to+download+ERA5.
 381 ERA5 hourly re-analysis output is also archived at the Copernicus Climate Data Store
 382 (data.marine.copernicus.eu/products) under the DOIs: 10.24381/cds.adbb2d47 (for
 383 single-level variables) and 10.24381/cds.bd0915c6 (for multi-level variables). The
 384 WAIS 1080 model set-up, as well as an explanation of how to set up the tracer release
 385 experiments, is available at: doi.org/10.5281/zenodo.6842019. RTopo-2 bathymetry
 386 (Schaffer & Timmermann, 2016) is available from Pangaea (www.pangaea.de) with
 387 the DOI: 10.1594/PANGAEA.856844. Data processing and figure preparation were
 388 carried out using Matlab R2021a.

389 Acknowledgements

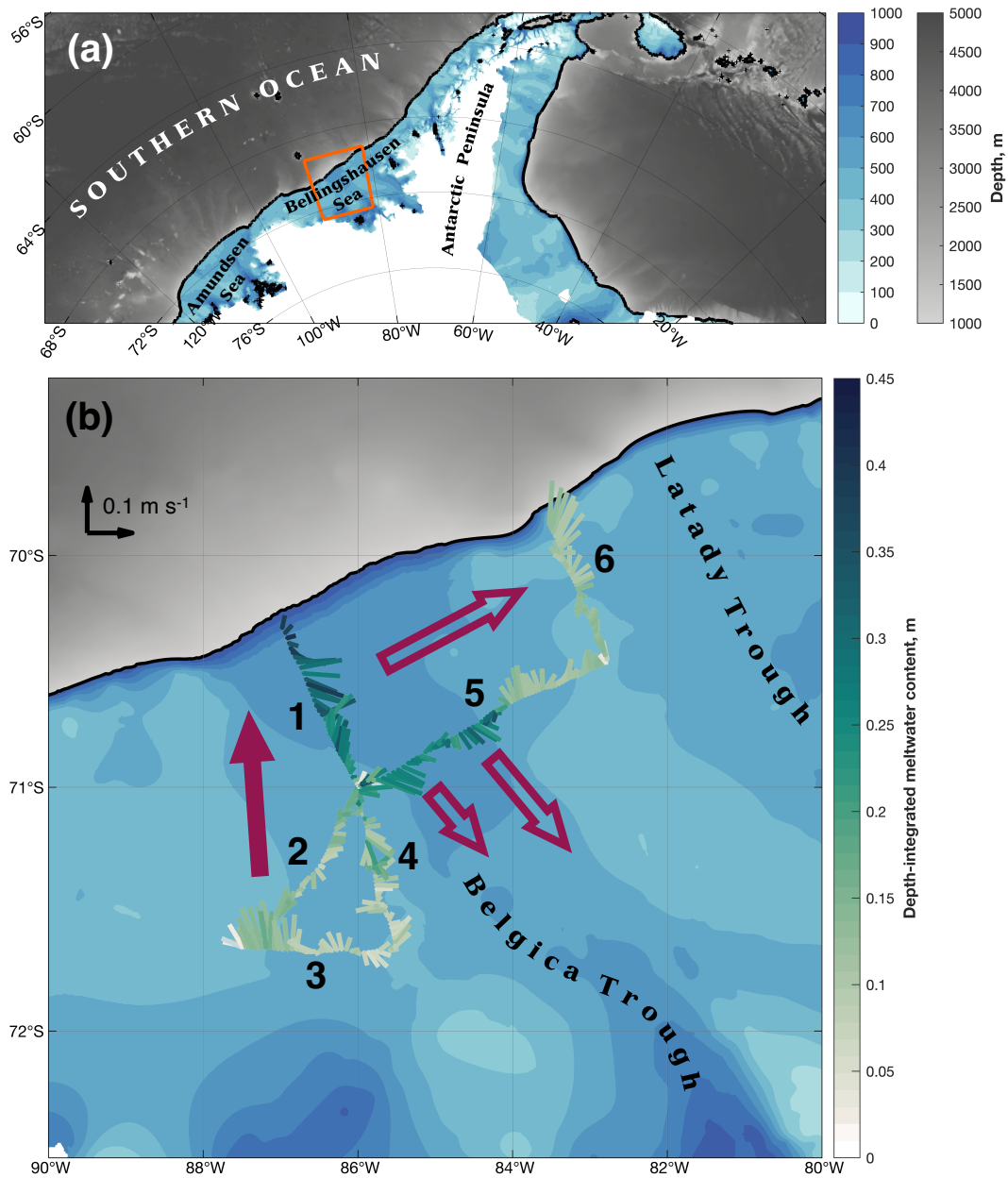
390 PMFS and KJH were supported by the COMPASS project (grant number 741120),
 391 which was funded by the European Research Council under the Horizon 2020 program.
 392 AFT and MMF were supported by NSF award OPP-1644172 and NASA Jet Propulsion
 393 Laboratory’s Research and Technical Development Earth 2050 project. The work of
 394 MPS was carried out at the Jet Propulsion Laboratory under a contract with NASA.
 395 We gratefully acknowledge support from the NASA Cryospheric Sciences Program.
 396 High-end computing resources were provided by the NASA Advanced Supercomputing
 397 Division of the Ames Research Center.

398 References

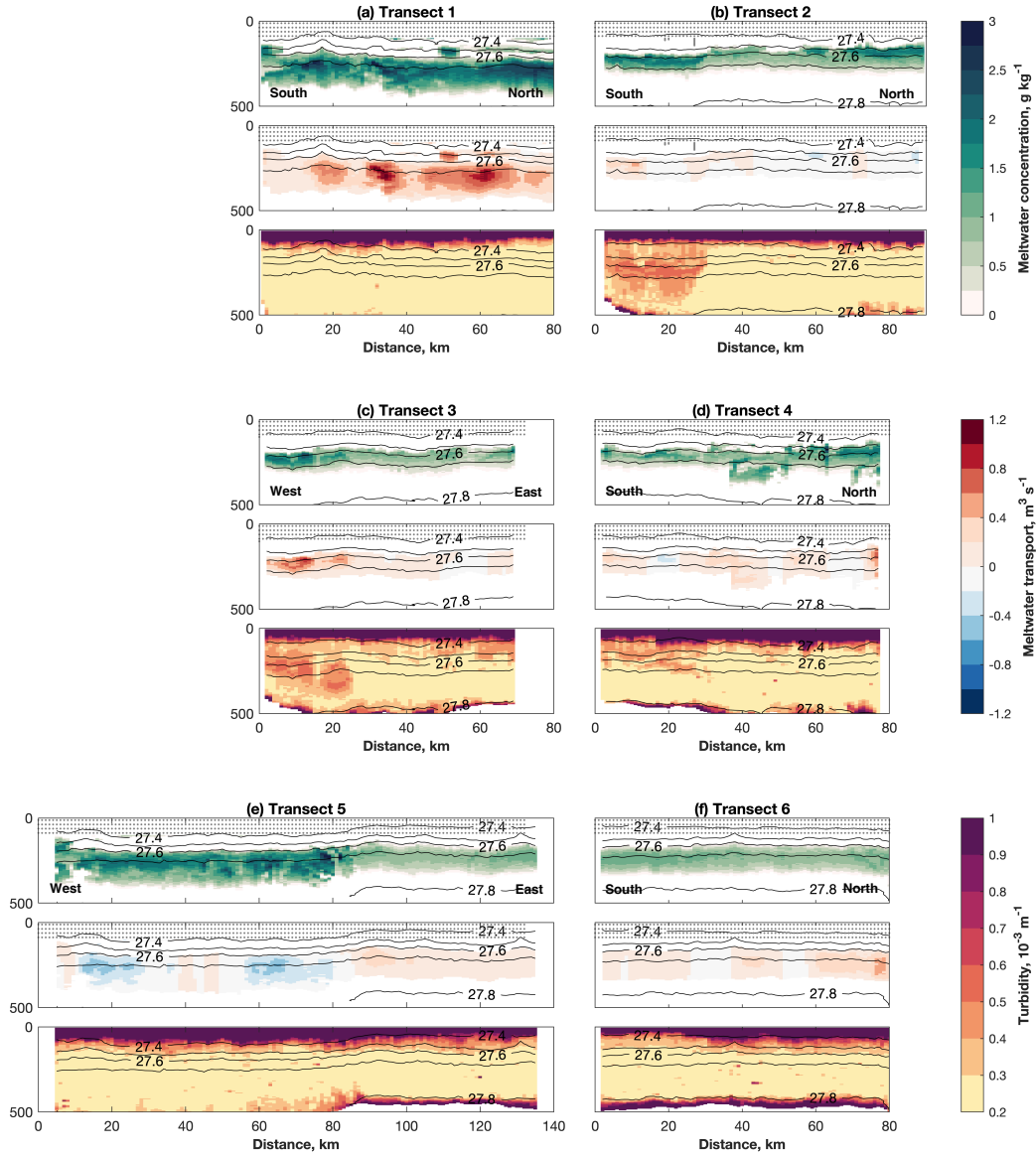
- 399 Biddle, L. C., Heywood, K. J., & Kaiser, J. (2017). Glacial meltwater identification in the
 400 Amundsen Sea. *Journal of Physical Oceanography*, 47, 933 – 954.
- 401 Dawson, H. R. S., Morrison, A. K., England, M. L., & Tamsitt, V. (2023). Pathways and
 402 timescales of connectivity around the Antarctic continental shelf. *Journal of*
 403 *Geophysical Research: Oceans*, 128, e2022JC018962.
- 404 Donat-Magnin, M., Jourdain, N. C., Spence, P., Le Sommer, J., Gallée, H., & Durand, G.
 405 (2017). Ice-shelf melt response to changing winds and glacier dynamics in the
 406 Amundsen Sea sector, Antarctica. *Journal of Geophysical Research: Oceans*, 122,
 407 10206 – 10224.
- 408 Flexas, M. M., Thompson, A. F., Schodlok, M. P., Zhang, H., & Speer, K. (2022).
 409 Antarctic Peninsula warming triggers enhanced basal melt rates throughout West
 410 Antarctica. *Science Advances*, 8, eabj9134.
- 411 Forget, G., Campin, J. M., Heimbach, P., Hill, C. N., Ponte, R. M., & Wunsch, C. (2015).
 412 ECCO version 4: an integrated framework for non-linear inverse modelling and
 413 global ocean state estimation. *Geoscientific Model Development*, 8, 3071 – 3104.
- 414 Frajka-Williams, E., Eriksen, C. C., Rhines, P. B., & Harcourt, R. R. (2011).
 415 Determining vertical water velocities from Seaglider. *Journal of Atmospheric and*
 416 *Oceanic Technology*, 28, 1641 – 1656.
- 417 Garau, B., Ruiz, S., Zhang, W. G., Pascual, A., Heslop, E., Kerfoot, J., & Tintoré, J.
 418 (2011). Thermal lag correction on Slocum CTD glider data. *Journal of Atmospheric*
 419 *and Oceanic Technology*, 28, 1065 – 1071.
- 420 Green, R. E., Bower, A. S., & Lugo-Fernández. (2014). First autonomous bio-optical
 421 profiling float in the Gulf of Mexico reveals dynamic biogeochemistry in deep waters.
 422 *PLOS One*, 9, e101658.
- 423 Gunn, K. L., White, N. J., Larter, R. D., & Caulfield, C. P. (2018). Calibrated seismic

- 424 imaging of eddy-dominated warm-water transport across the Bellingshausen Sea,
 425 Southern Ocean. *Journal of Geophysical Research: Oceans*, *123*, 3072 – 3099.
- 426 Hersbach, H., Bell, B., Berrisford, P., Hirahara, S., Horányi, A., Muñoz-Sabater, J., ...
 427 Thépaut, J.-N. (2020). The ERA5 global re-analysis. *Quarterly Journal of the Royal*
 428 *Meteorological Society*, *146*, 1999 – 2049.
- 429 Jacobs, S. S., & Giulivi, C. F. (2010). Large multidecadal salinity trends near the
 430 Pacific-Antarctic continental margin. *Journal of Climate*, *23*, 4508 – 4524.
- 431 Jenkins, A. (1999). The impact of melting ice on ocean waters. *Journal of Physical*
 432 *Oceanography*, *29*, 2370 – 2381.
- 433 Jenkins, A., & Jacobs, S. (2008). Circulation and melting beneath George VI Ice Shelf,
 434 Antarctica. *Journal of Geophysical Research: Oceans*, *113*, C04013.
- 435 Jenkins, A., Shoosmith, D., Dutrieux, P., Jacobs, S., Kim, T. W., Lee, S. H., ...
 436 Stammerjohn, S. (2018). West Antarctic Ice Sheet retreat in the Amundsen Sea
 437 driven by decadal oceanic variability. *Nature Geoscience*, *11*, 733 – 738.
- 438 Kim, T.-W., Yang, H. W., Dutrieux, P., Wåhlin, A. K., Jenkins, A., Kim, Y. G., ... Cho,
 439 Y.-K. (2021). Interannual variation of Modified Circumpolar Deep Water in the
 440 Dtoson-Getz Trough, West Antarctica. *Journal of Geophysical Research: Oceans*,
 441 *126*, e2021JC017491.
- 442 Kimura, S., Jenkins, A., Regan, H., Holland, P. R., Assmann, K. M., Whitt, D. B., ...
 443 Dutrieux, P. (2017). Oceanographic controls on the variability of ice-shelf basal
 444 melting and circulation of glacial meltwater in the Amundsen Sea Embayment,
 445 Antarctica. *Journal of Geophysical Research: Oceans*, *122*, 10131 – 10155.
- 446 Lago, V., & England, M. L. (2019). Projected slowdown of Antarctic Bottom Water in
 447 response to amplified meltwater contributions. *Journal of Climate*, *32*, 6319 – 6335.
- 448 Lee, G. A., Damerell, G. M., Heywood, K. J., Oelerich, R., Azaneu, M., Flexas, M. M., ...
 449 Zheng, Y. (2022). Seaglider observations in the Belgica Trough and over the
 450 continental slope of the Bellingshausen Sea, Antarctica, February to March 2020.
 451 *British Oceanographic Data Centre, National Oceanography Centre, NERC, DOI:*
 452 *10.5285/ea24b8e5-b10e-68bf-e053-6c86abc06c97*,
 453 [www.bodc.ac.uk/data/published_data_library/catalogue/10.5285/ea24b8e5-b10e-](http://www.bodc.ac.uk/data/published_data_library/catalogue/10.5285/ea24b8e5-b10e-68bf-e053-6c86abc06c97/)
 454 [68bf-e053-6c86abc06c97/](http://www.bodc.ac.uk/data/published_data_library/catalogue/10.5285/ea24b8e5-b10e-68bf-e053-6c86abc06c97/).
- 455
- 456 Moffat, C., Owens, B., & Beardsley, R. C. (2009). On the characteristics of Circumpolar
 457 Deep Water intrusions to the west Antarctic Peninsula continental shelf. *Journal of*
 458 *Geophysical Research*, *114*, C05017.
- 459 Morlighem, M., Rignot, E., Binder, B. D. D., T., Drews, R., Eagles, G., Eisen, O., ...
 460 Young, D. A. (2020). Deep glacial troughs and stabilising ridges unveiled beneath
 461 the margins of the Antarctic ice sheet. *Nature Geoscience*, *13*, 132 – 137.
- 462 Nakayama, Y., Menemenlis, D., Schodlok, M., & Rignot, E. (2017). Amundsen and
 463 Bellingshausen Seas simulation with optimised ocean, sea ice and thermodynamic ice
 464 shelf model parameters. *Journal of Geophysical Research: Oceans*, *122*, 6180 – 6195.
- 465
- 466 Nakayama, Y., Menemenlis, D., Zhang, H., Schodlok, M., & Rignot, E. (2018). Origin of
 467 Circumpolar Deep Water intruding onto the Amundsen and Bellingshausen Sea
 468 continental shelves. *Nature Communications*, *9*, 3403.
- 469 Nakayama, Y., Timmermann, R., B., R. C., M., S., & Hellmer, H. H. (2014). Modelling
 470 the spreading of glacial meltwater from the Amundsen and Bellingshausen Seas.
 471 *Geophysical Research Letters*, *41*, 7942 – 7949.
- 472 Nakayama, Y., Timmermann, R., & Hellmer, H. H. (2020). Impact of West Antarctic ice
 473 shelf melting on Southern Ocean hydrography. *The Cryosphere*, *14*, 2205 – 2216.
- 474 Oelerich, R., Heywood, K. J., Damerell, G. M., & Thompson, A. F. (2022). Wind-induced
 475 variability of warm water on the southern Bellingshausen Sea continental shelf.
 476 *Journal of Geophysical Research: Oceans*, *127*, e2022JC018636.
- 477 Orsi, A. H., Whitworth, T., & Nowlin Jnr., W. D. (1995). On the meridional extent and
 478 fronts on the Antarctic Circumpolar Current. *Deep-Sea Research I*, *42*, 641 – 673.

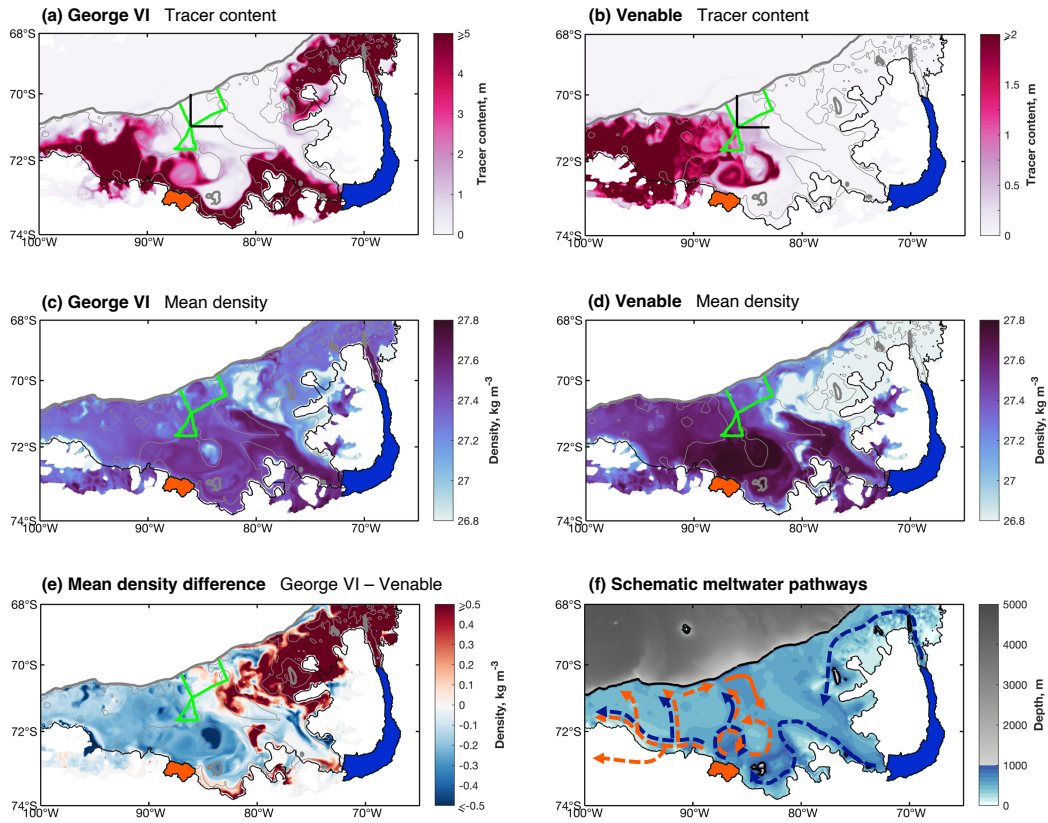
- 479 Padman, L. H., Costa, D. P., Bolmer, S. T., Goebel, M. E., Huckstadt, L. A., Jenkins, A.,
480 ... Shoosmith, D. R. (2010). Seals map bathymetry of the Antarctic continental
481 shelf. *Geophysical Research Letters*, *37*, L21601.
- 482 Padman, L. H., Erofeeva, S. Y., & Fricker, H. A. (2008). Improving Antarctic tide models
483 by assimilation of ICESat laser altimetry over ice shelves. *Geophysical Research
484 Letters*, *35*, L22504.
- 485 Padman, L. H., Fricker, H. A., Coleman, R., Howard, S., & Erofeeva, S. Y. (2002). A new
486 tide model for the Antarctic ice shelves and seas. *Annals of Glaciology*, *34*,
487 247 – 254.
- 488 Rignot, E., Mouginot, J., Scheuchl, B., van den Broeke, M., van Wessem, M. J., &
489 Morlighem, M. (2019). Four decades of Antarctic ice sheet mass balance from 1979
490 to 2017. *Proceedings of the National Academy of Sciences of the United States of
491 America*, *116*, 1095 – 1103.
- 492 Ruan, X., Speer, K. G., Thompson, A. F., Schulze Chretien, L. M., & Shoosmith, D. R.
493 (2021). Ice-shelf meltwater overturning in the Bellingshausen Sea. *Journal of
494 Geophysical Research: Oceans*, *126*, e2020JC016957.
- 495 Schaffer, J., & Timmermann, R. (2016). Greenland and Antarctic ice sheet topography,
496 cavity geometry and global bathymetry, (Rtopo-2). *Pangaea*,
497 doi.org/10.1594/PANGAEA.856844.
- 498 Schubert, R., Thompson, A. F., Speer, K., Schulze Chretien, L., & Bebieva, Y. (2021).
499 The Antarctic Coastal Current in the Bellingshausen Sea. *The Cryosphere*, *15*,
500 4179 – 4199.
- 501 Schulze Chretien, L. M., Thompson, A. F., Flexas, M. M., Speer, K., Swaim, N., Oelerich,
502 R., ... LoBuglio, C. (2021). The shelf circulation of the Bellingshausen Sea. *Journal
503 of Geophysical Research: Oceans*, *126*, e2020JC016871.
- 504 Silvano, A., Rintoul, S. R., Peña-Molino, B., Hobbs, W. R., van Wijk, E., Aoki, S., ...
505 Williams, G. D. (2018). Freshening by glacial meltwater enhances melting of ice
506 shelves and reduces formation of Antarctic Bottom Water. *Science Advances*, *4*,
507 eaap9467.
- 508 Thompson, A. F., Speer, K. G., & Schulze Chretien, L. M. (2020). Genesis of the
509 Antarctic Slope Current in West Antarctica. *Geophysical Research Letters*, *47*,
510 e2020GL087802.
- 511 Thompson, A. F., Stewart, A. L., Spence, P., & Heywood, K. J. (2018). The Antarctic
512 Slope Current in a changing climate. *Reviews of Geophysics*, *56*, 741 – 770.
- 513 Thurnherr, A. M., Jacobs, S. S., Dutrieux, P., & Giulivi, C. F. (2014). Export and
514 circulation of ice cavity water in Pine Island Bay, West Antarctica. *Journal of
515 Geophysical Research: Oceans*, *119*, 1754 – 1764.
- 516 Wåhlin, A. K., Yuan, X., Björk, G., & Nohr, C. (2010). Inflow of warm Circumpolar
517 Deep Water in the central Amundsen shelf. *Journal of Physical Oceanography*, *40*,
518 1427 – 1434.
- 519 Whitworth, T., Orsi, A. H., Kim, S.-J., Nowlin, W. D., & Locarnini, R. A. (1998). Water
520 masses and mixing near the Antarctic Slope Front. In S. J. Jacobs & F. Weiss
521 (Eds.), *Ocean, ice, and atmosphere: Interactions at the Antarctic continental margin*
522 (pp. 1 – 27). Washington DC, United States of America: American Geophysical
523 Union.
- 524 Zhang, X., Thompson, A. F., Flexas, M. M., Roquet, F., & Bornemann, H. (2016).
525 Circulation meltwater distribution in the Bellingshausen Sea: from shelf break to
526 coast. *Geophysical Research Letters*, *43*, 6402 – 6409.
- 527 Zheng, Y., Heywood, K. J., Webber, B. G. M., Stevens, D. P., Biddle, L. C., Boehme, L.,
528 & Loose, B. (2021). Winter seal-based observations reveal glacial meltwater
529 surfacing in the southeastern Amundsen Sea. *Communications Earth &
530 Environment*, *2*, 40.
- 531 Zheng, Y., Stevens, D. P., Heywood, K. J., Webber, B. G. M., & Queste, B. Y. (2022).
532 Reversal of ocean gyres near ice shelves in the Amundsen Sea caused by the
533 interaction of sea ice and wind. *The Cryosphere*, *16*, 3005 – 3019.



534 **Figure 1.** (a) Bathymetric map of the Southern Ocean and Antarctic continental shelf in
 535 the region of the Antarctic Peninsula, with the region shown in panel (b) outlined in orange.
 536 (b) Dive-average currents (m s^{-1} ; key in top left) colored by depth-integrated meltwater content
 537 (m). Bathymetric shading is as in panel (a). Bold numbers indicate transect number and purple
 538 arrows approximate key flows based on dive-average currents; filled arrows indicate turbid flows,
 539 un-filled arrows indicate clear flows. In both panels, the 1000 m isobath is indicated by the thick
 540 black line. Bathymetry is from RTopo-2.



541 **Figure 2.** For each transect, *top panel*: meltwater concentration (g kg^{-1}); *middle panel*: meltwater
 542 transport ($\text{m}^3 \text{s}^{-1}$), where positive transport indicates northward or eastward flow; and
 543 *bottom panel*: turbidity (10^{-3} m^{-1}). Contours in all panels indicate potential density (kg m^{-3}).
 544 The orientation of each transect is indicated by the compass points given at each end of the top
 545 panel. Regions excluded from the meltwater calculations are indicated by the grey dots.



546 **Figure 3.** Depth-integrated tracer content (m) of tracers released under (a) George VI and
 547 (b) Venable; the black lines indicate the sections used to calculate tracer transport. Mean
 548 density (kg m^{-3}) of tracers released under (c) George VI and (d) Venable. (e) The difference in
 549 mean density between tracer released under George VI and Venable (George VI minus Venable).
 550 Variables in panels (a) to (e) are averages over March 2020; densities are plotted only over the
 551 continental shelf. (f) Schematic of meltwater transport pathways. Meltwater from George VI
 552 is represented by the blue arrows; meltwater from Venable is represented by the orange arrows.
 553 Regions between the 500 and 1000 m isobaths are shaded light gray. In all panels: the ice edge
 554 is indicated by the black line and the 1000 m isobath by the thick gray line. In panels (a) to (e),
 555 the 500 m isobath is indicated by the thin gray line and the glider path is indicated by the green
 556 line. George VI and Venable ice shelves are colored blue and orange respectively. Bathymetry is
 557 from RTopo-2.